J. Fluid Mech. (1992), *vol.* 236, *pp.* 607–633
Printed in Great Britain

Numerical investigation of the high-speed conical flow past a sharp fin

By ARGYRIS G. PANARAS†
DLR, Bunsenstrasse 10, Göttingen, Germany

(Received 2 January 1991 and in revised form 8 July 1991)

The supersonic flow past a fin mounted on a flat plate is simulated numerically by solving the Reynolds averaged Navier–Stokes equations. The results agree well with the experimental data. Post-processing of the numerical solution provides the missing flow-field evidence for confirming the currently accepted flow model, whose conception was based mainly on surface data. It is found that the flow is dominated by a large vortical structure, which lies on the plate and whose core has a remarkably conical shape with flattened elliptical cross-section. Along the fin and close to the corner, a slowly growing smaller vortex develops. On top of the conical vortex and along it a λ-shock is formed. Quantitative data are presented, which show that the flow is not actually purely conical but a small deviation exists, especially at the part between the separation shock and the plate. This deviation is detected when the streamwise extent of the flow is more than 20–30 initial boundary-layer thicknesses. Owing to the rather quasi-conical nature of the flow, the various flow variables do not remain constant along rays that start at the origin of the conical flow field, but they vary slowly. Data are presented which support the view that this deviation from conical bchaviour is mainly due to the effect of the smaller rate of development of the boundary later of the plate, compared to the conical vortex.

1. Introduction

The impingement of a shock wave on the boundary layer developing along a surface is one important three-dimensional interaction, which may have significant influence on the performance of some parts of a hypersonic vehicle, like its intakes and its control surfaces, owing to the localized high pressure and heat transfer rates that usually accompany these types of flow. Traditionally the impinging shock is called a glancing shock, to distinguish it from the case of a generation of a shock wave on the same surface on which the boundary layer develops.

Various simple geometries have been studied, both experimentally and computationally, that resemble elements of a hypersonic vehicle subjected to a glancing shock-wave/turbulent-boundary-layer interaction. The attachment of a sharp fin normally to a flat plane is one of the rather simple configurations which result in such an interaction. The oblique shock that is generated on the fin crosses the boundary layer, which grows along the plate, and owing to the subsonic part of the latter, the shock pressure increase is smeared out on the wall, so that a disturbed flow pattern appears which covers a significant part of the flow upstream and downstream of the inviscid shock position. If the shock is sufficiently strong the flow separates and the

† Present address: Agias Elenis 63, Athens 15772, Greece.

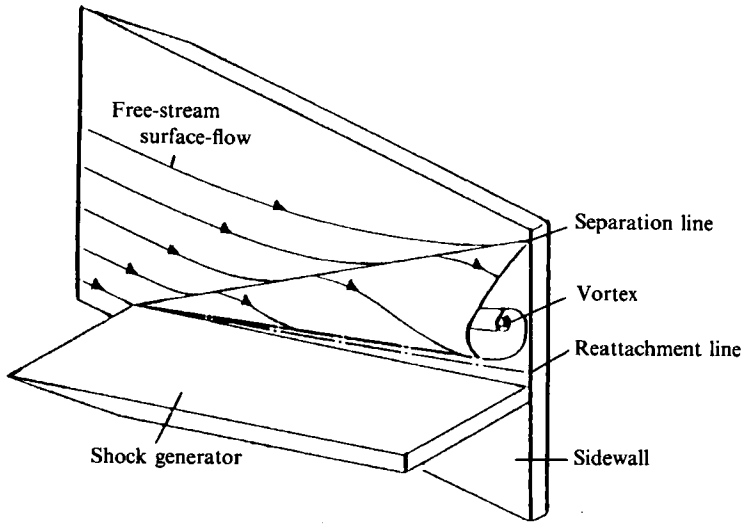

FIGURE 1. Flow field model proposed by Token (1974).

topology of the flow changes significantly. Numerous studies, most of them experimental, have been performed over the last 20 years using the fin–plate or the compression-corner configuration, whose flow structure is similar. Surface flow visualization and pressure measurements have provided the basic information for the determination of the type of flow established. The contributions of Maskell (1955) and Lighthill (1963), on determining the topology of three-dimensional separation from surface observations have been very helpful here.

The first flow model of the fin–plate configuration was proposed by Token (1974). In an attempt to explain the strong peaks in the heat transfer near the fin–plate junction, Token suggested that a separation vortex appears between a separation line visible on the flat plate just ahead of the shock, and a reattachment line also on the flat plate but close to the corner (figure 1). More recently, Kubota & Stollery (1982) have improved the model of Token after carrying out an extensive experimental programme for variable shocks at a Mach number of 2.3. In addition to surface measurements, they have done a series of vapour and smoke-screen studies that helped to detect a smaller vortical structure that appears on the surface of the fin, close to the corner. This small structure is always present, according to Kubota & Stollery, even when a weak interaction is established (figure 2*a*). If the interaction is strong, the separated flow is made up of two vortices: a tight, vigorous, roughly circular one in the corner, with a weak, elongated one above it (figure 2*b*). For the test conditions of Kubota & Stollery, the size and shape of the vortices were such that they occupied a region equal to the initial boundary thickness, even at the trailing-edge position of the fin. However, they note that the vortices would be expected to grow and thus have a larger effect on the outer flow further downstream. Both proposed models indicate that the large vortex develops conically (figures 1, 2*b*). This feature is based on the observation that on the surface of the plate the separation and reattachment lines converge towards a virtual origin ahead of the fin.

Subsequent studies have confirmed the quasi-conical nature of the fin-plate interaction (e.g. Settles & Dolling 1986; Shapey & Bogdonoff 1987). It has been found that in addition to the separation and reattachment lines, the extrapolation

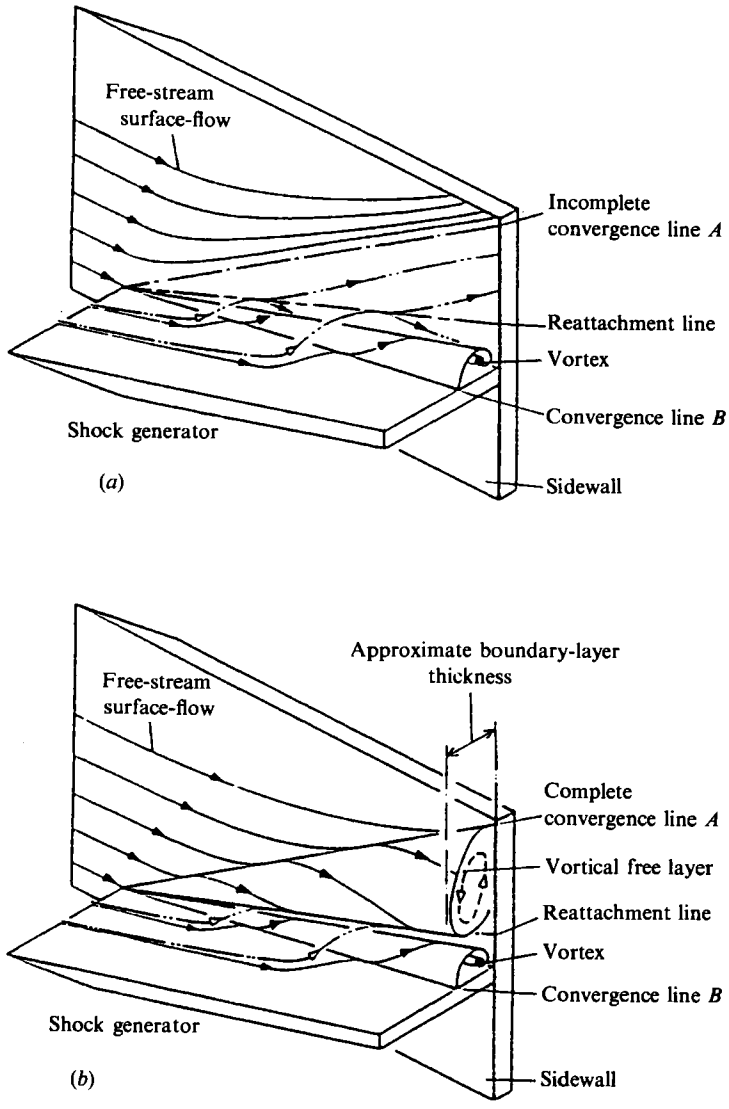

FIGURE 2. Flow field model proposed by Kubota & Stollery (1982): (*a*) weak interaction; (*b*) strong interaction.

of the undisturbed oblique shock wave also converges approximately to the virtual conical origin. There is only a systematic deviation from conical behaviour in the vicinity of the fin's leading edge, in a region called the 'inception zone' (Lu & Settles 1989). An important consequence of the quasi-conical nature of these interactions is the presumption that their features are entirely projected upon the surface of a sphere whose origin is the virtual conical origin (Alvi & Settles 1990). That is because no change occurs along the rays of a conical flow. Alvi & Settles (1990) have demonstrated this feature of the conical flow. Focusing a light beam at the virtual origin of the approximate conical flow field and aiming it such that the resulting conical light beam coincided with the rays of the swept interaction (conical shadowgraphy), they obtained pictures whose interpretation leads to the modified interaction flow-field model shown in figure 3. This model includes, in addition to the

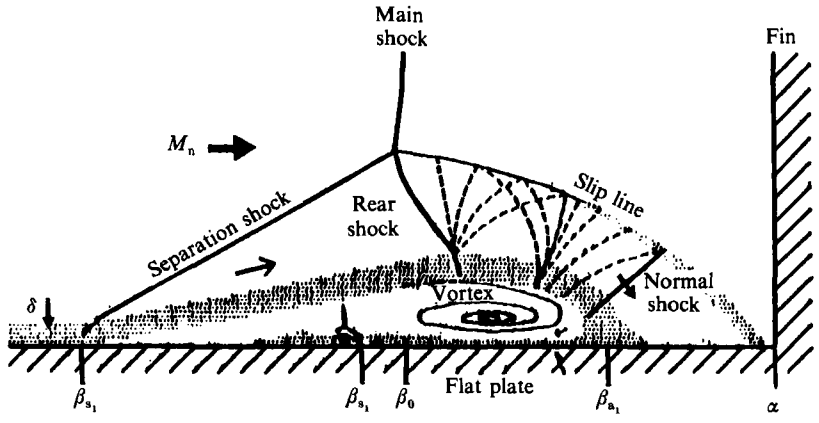

FIGURE 3. Modified model of Alvi & Settles (1990).

λ-shock structure, evidence of the so-called secondary separation and the appearance of a normal shock in the region of impingement of the air, after it passes through the λ-shock system. According to Alvi & Settles (1990), the secondary separation appears only for moderate strength interactions and not for weak or very strong ones.

Evidently, in addition to the experimental studies, numerical simulations are needed to provide more details of the flow structure away from the walls. Actually, the fin–plate configuration and the compression-corner flow, have been objects of numerical studies since the early days of numerical simulation of viscous flows (e.g. Hung & MacCormack 1977; Horstman & Hung 1979). A systematic computational program in this field has been applied by D. Knight and C. Horstman in cooperation with S. Bogdonoff. Their latest results, which are related to a strong fin–plate interaction, are reported by Knight *et al.* (1987). The computed surface and Pitot pressure, as well as the yaw angle profiles and the surface streamlines, are observed in good agreement with the experimental data, thereby confirming the efficiency of their codes. Concerning the existence of the conical vortex, they have found that the trajectories of streamlines that originate upstream of the separation line close to the wall rise, cross the separation line and rotate in the direction in which the separation vortex should rotate. This supplies strong evidence that the model of Kubota & Stollery (1982) is correct. However, direct visual evidence of the existence of the conical vortex structure, of the smaller vortex along the fin and of the associated shock system is still missing. Besides, no data have been presented which quantitatively support the hypothesis of the conical nature of the flow.

The purpose of this study is to provide the missing vital evidence of the establishment of a quasi-conical flow field in a fin–plate configuration. To this end, an existing thin-layer Navier–Stokes code (Müller 1990) was modified, so that all the viscous terms are retained in the directions normal to the plate and to the fin. This modification is necessary for an accurate simulation of the particular flow. Attention has been given to the grid refinement and to the use of an efficient technique for the visual detection of three-dimensional vortices. The code uses an upwind TVD scheme, which is known to capture the shock waves very efficiently.

2. Description of the numerical procedure

2.1. *Equations and numerical method*

The governing Navier–Stokes equations in dimensionless conservation law form and in general coordinates are

$$\frac{\partial \boldsymbol{Q}}{\partial \tau}+\frac{\partial \boldsymbol{E}}{\partial \xi}+\frac{\partial \boldsymbol{F}}{\partial \eta}+\frac{\partial \boldsymbol{G}}{\partial \zeta}=\frac{\partial \boldsymbol{E}_{\mathrm{v}}}{\partial \xi}+\frac{\partial \boldsymbol{F}_{\mathrm{v}}}{\partial \eta}+\frac{\partial \boldsymbol{G}_{\mathrm{v}}}{\partial \zeta}, \tag{1}$$

where $\boldsymbol{Q}=J^{-1}(\rho,\rho u,\rho v,\rho w,e)^{\mathrm{T}}$ is the vector of the conservative variables, and J is the Jacobian of the transformation from Cartesian to general coordinates. $\boldsymbol{E},\boldsymbol{F},\boldsymbol{G}$ are the inviscid and $\boldsymbol{E}_{\mathrm{v}},\boldsymbol{F}_{\mathrm{v}},\boldsymbol{G}_{\mathrm{v}}$ are the viscous fluxes in the streamwise ξ-, lateral η-, and normal ζ-direction correspondingly. The expressions for the fluxes are given in certain textbooks.

Stokes' hypothesis is used for relating the two viscosity coefficients, which appear in the viscous fluxes. Also, the Sutherland law is employed for the estimation of the molecular viscosity. The above system of equations is valid for laminar as well as turbulent flows, by replacing the molecular transport coefficients with their turbulent counterparts. The turbulence model is described in §2.4.

In the original version of the numerical algorithm which was used in the present study (Müller 1990), the thin-layer approximation is applied, according to which the viscous terms are retained only in the direction normal to the wall. In the case of the fin–plate configuration, walls exist in two directions (η and ζ). Thus, it is necessary to apply the concept of the thin-layer approximation to both of them. Furthermore, in the corner region, the viscous terms associated with cross-derivatives may be of the same order of magnitude as the normal derivatives, which are the only ones retained in the thin-layer approximation. Considering these facts the code of Müller was modified, so that in the directions of the two walls all the viscous terms were retained.

Equations (1) are solved at the interior grid points of a boundary-fitted structured mesh. A second-order central differencing is applied to the implicitly treated viscous fluxes. The inviscid fluxes are determined by the upwind total variational diminishing (TVD) scheme of Yee & Hartem (1987), which uses Roe's approximate Riemann solver (Roe 1981) and Harten's second-order modified flux approach. Employing the first-order Euler implicit formula, the inviscid fluxes are approximately linearised. Since the resulting linear system is block-diagonally dominant with respect to the spectral radii, it may be solved by a relaxation method. In the present case, where time marching was applied for calculating the steady-flow solution, alternating Gauss–Seidel relaxation in the streamwise direction was employed.

2.2 *Computational mesh*

Owing to the simplicity of the geometry of the fin–plate configuration, the mesh was generated algebraically. For an adequate resolution of the viscous effects a clustering was applied close to the plate and to the fin. In figure 4 the mesh which was used is shown. In each crossflow plane (z-, y-directions) 95×79 points were used, while in the streamwise x-direction there were 45 grid planes uniformly spaced, with $\Delta x=\delta_\infty$. The input plane was located at a distance equal to $2\delta_\infty$ upstream of the leading edge of the fin, and the downstream boundary at $x=43\delta_\infty$. The height of the computational domain was $11\delta_\infty$. The width was uniform before the fin, equal to $10\delta_\infty$, but from there on it increased to $z=43\delta_\infty$ at the outflow plane. This widening was necessary

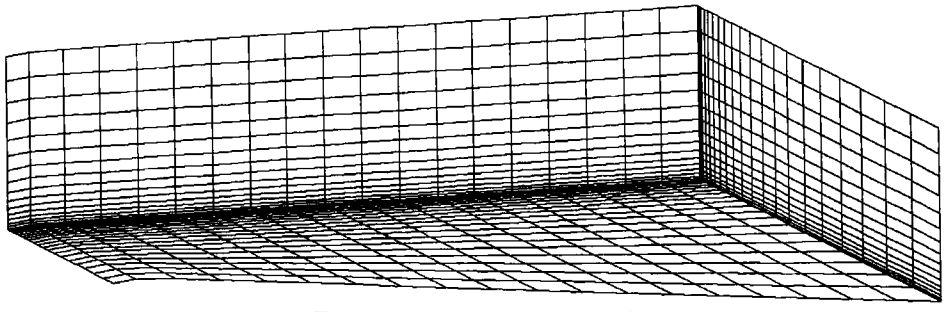

FIGURE 4. Computational grid.

to ensure that the computational domain laterally extended more than the interaction domain (for the application of the boundary conditions). Previously a solution had been obtained whose axial spacing was half of the final one, but it extended only to $x = 37\delta_\infty$. For that solution a two-zones approach had been applied. Both solutions provided results of the same accuracy. It seems that the fineness of the grid at the crossflow planes is more important for the fin–plate configuration than in the axial direction.

It is noted that the axial extent of the calculated flow field is almost three times longer than the extent of the experimental flow which the present calculations simulate. The longer extent is necessary to study the development of the vortex far from the origin of the conical flow.

2.3 *Boundary conditions*

A boundary-layer profile, having equal thickness and Reynolds number to the experimental one, was prescribed at the inflow plane. This profile was also used as the initial condition of the flow field. On the outflow boundary, as well as on the far field (upper and lateral boundaries) the gradients of the flow were set equal to zero. The wall was assumed impermeable, and no-slip boundary conditions were applied. Also, the wall was assumed adiabatic and the pressure gradient normal to the wall was set to zero. On the symmetry boundary (upstream of the fin, at $z = 0$) the normal component of the velocity was set to zero, while the normal derivatives of the remaining flow quantities were assumed to be zero.

2.4. *Turbulence model*

One important conclusion of the numerical study of Knight *et al.* (1987) was that the overall structure of the three-dimensional sharp fin interaction is insensitive to the turbulence model, except within a small portion of the boundary layer adjacent to the surface. This conclusion is based on the fact that though Knight *et al.* used two different turbulence models (i.e. the algebraic eddy viscosity model of Baldwin & Lomax (1978) and the k-ϵ model) which resulted in significant differences in the turbulent eddy viscosity profiles, the velocity fields computed by both models were in close agreement.

Considering the computational simplicity which an algebraic model offers, it was decided to use in the present calculations the two-layer model developed by Baldwin & Lomax (1978). This model is similar to the Cebeci and Smith model, but with modifications that avoid the necessity of finding the edge of the boundary layer.

The calculation of the eddy viscosity is done in the crossflow planes ((y, z)-planes), for successive streamwise positions (x-direction). In each (y, z)-plane, the com-

putational domain is an orthogonal rectangle formed by the plate and by the fin. In the inner region the Prandtl–Van Driest formulation is used

$$(\mu_t)_{\text{inner}} = \rho(\kappa D\eta)^2\omega. \tag{2}$$

where κ is the von Kármán constant, D is the van Driest damping factor, ω is the magnitude of the vorticity and η is the distance normal to the wall. In the particular case examined here, where there are two walls, a modified distance developed by Hung & MacCormack (1978) is used:

$$\eta = \frac{2yz}{y+z+(y^2+z^2)^{\frac{1}{2}}}. \tag{3}$$

This modified distance accounts for the turbulent mixing length near the corner under the influence of both walls. In the outer region, the following equation is used

$$(\mu_t)_{\text{outer}} = C_{\text{cp}}(0.0168\rho F_{\text{wake}}\beta), \tag{4}$$

$$F_{\text{wake}} = \text{the smaller of} \begin{cases} \eta_{\max} F_{\max}, \\ C_{\text{wk}}\,\eta_{\max}\,u_{\text{dif}}^2/F_{\max} \end{cases}.$$

The quantity $F_{\max}$ is the maximum value of the function $F(\eta) = \eta\omega D$, and $\eta_{\max}$ is the value of η at which it occurs. The Klebanoff intermittency factor β is given by

$$\beta = \left[1+5.5\left(\frac{C_{\text{Kleb}}\,\eta}{\eta_{\max}}\right)^6\right]^{-1}. \tag{5}$$

The quantity u_{dif} is the difference between the maximum and minimum velocity in the profile (in the present case it is equal to u_e). The constants appearing in the previous relations are $C_{\text{cp}} = 1.6$, $C_{\text{wk}} = 0.25$, $C_{\text{Kleb}} = 0.3$.

3. Results

The flow which has been studied experimentally by Shapey & Bogdonoff (1987) and numerically by Knight *et al.* (1987), has been selected to be simulated numerically. The flow has $M_\infty = 2.94$, $Re_\delta = 8.8\times10^5$, and $\alpha = 20°$. There is only one lengthscale in the flow: the thickness of the boundary layer upstream of the fin. Its value in the case studied is $\delta_\infty = 1.27$ cm. Using the freestream data we have calculated a boundary-layer velocity profile, which we have used for the determination of the initial flow conditions at the start of the calculations. Subsequently, this velocity profile was kept constant only at the input plane. In the following section, comparisons of the calculated flow field with experimental data are presented, which show that the flow studied is adequately simulated. Then visual images of the flow are presented, which reveal the vortex system and the accompanying shock structure. After that, the conical nature of the flow field is investigated quantitatively.

3.1. *Comparison with experiments*

Shapey & Bogdonoff (1987) have obtained surface pressure distributions along rows of orifices aligned with the flow direction. Also, the boundary layer on the flat plane (which in this case was the wind-tunnel wall) was surveyed using a computer-controlled cobra probe. In addition to the Pitot pressure (P_T), the probe measured the yaw angle β, where $\beta = \tan^{-1}(w/u)$ and u, v, w are the Cartesian components of the

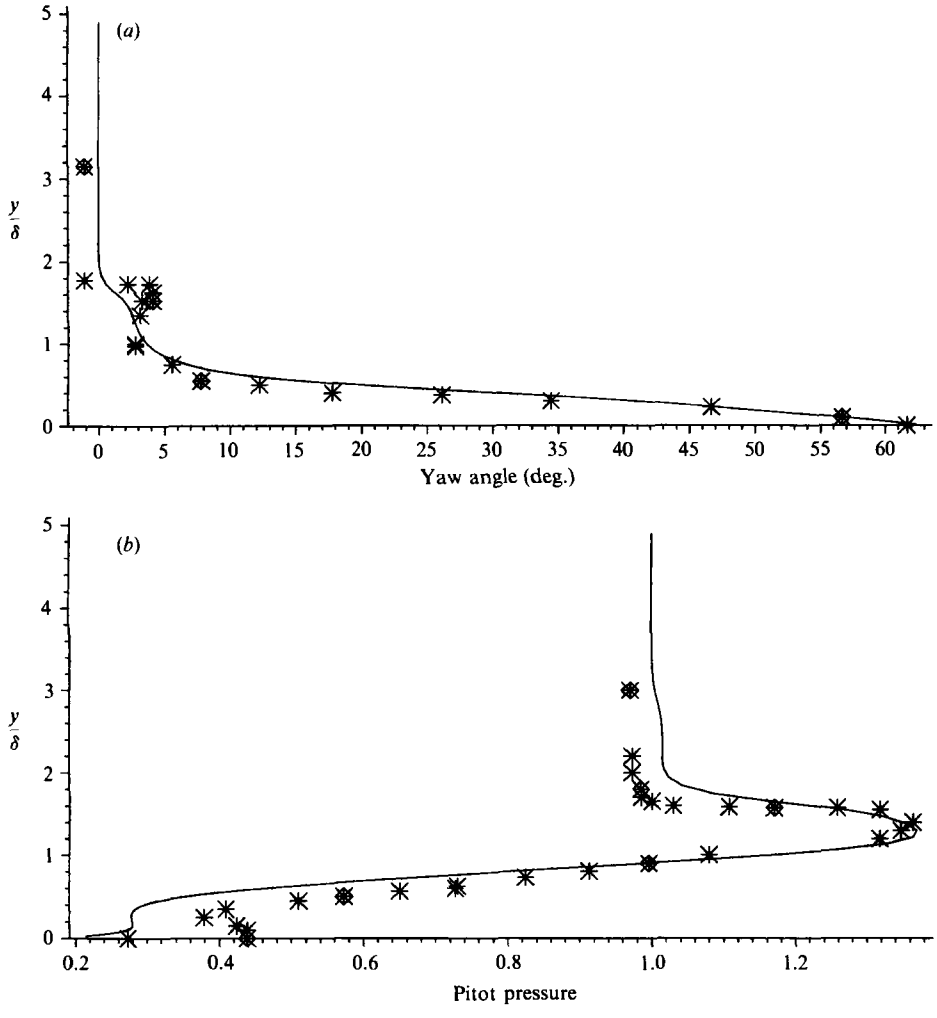

FIGURE 5. Comparison of calculated and measured Pitot pressure and yaw angle at Station 5: (*a*) yaw angle; (*b*) Pitot pressure.

velocity in the x-, y-, z-directions. The alignment of the survey positions with the flow direction was a good choice, because the data cover a zone that starts in the upstream undisturbed flow area, crosses the separation line, passes through the λ-shock and terminates close to the fin after crossing the reattachment line.

In figure 5, the comparison is shown between the computed and the measured yaw angle and the Pitot pressure at Station 5, which is located between the separation line and the shock, with one undisturbed boundary-layer thickness upstream of the shock. The Pitot pressure has been normalized by the freestream Pitot pressure. All lengths are normalized by the thickness of the undisturbed boundary layer. It is observed, in figure 5, that the agreement between the calculated profiles and the experimental ones is very good. The 'overshoot' of the Pitot pressure above the boundary layer is due to the compression system ahead of the shock.

In figure 6 the same quantities, β and P_T, are compared at Station 7, which is located approximately half a boundary-layer thickness downstream of the inviscid shock position. Again the agreement is very good, especially in the case of the yaw

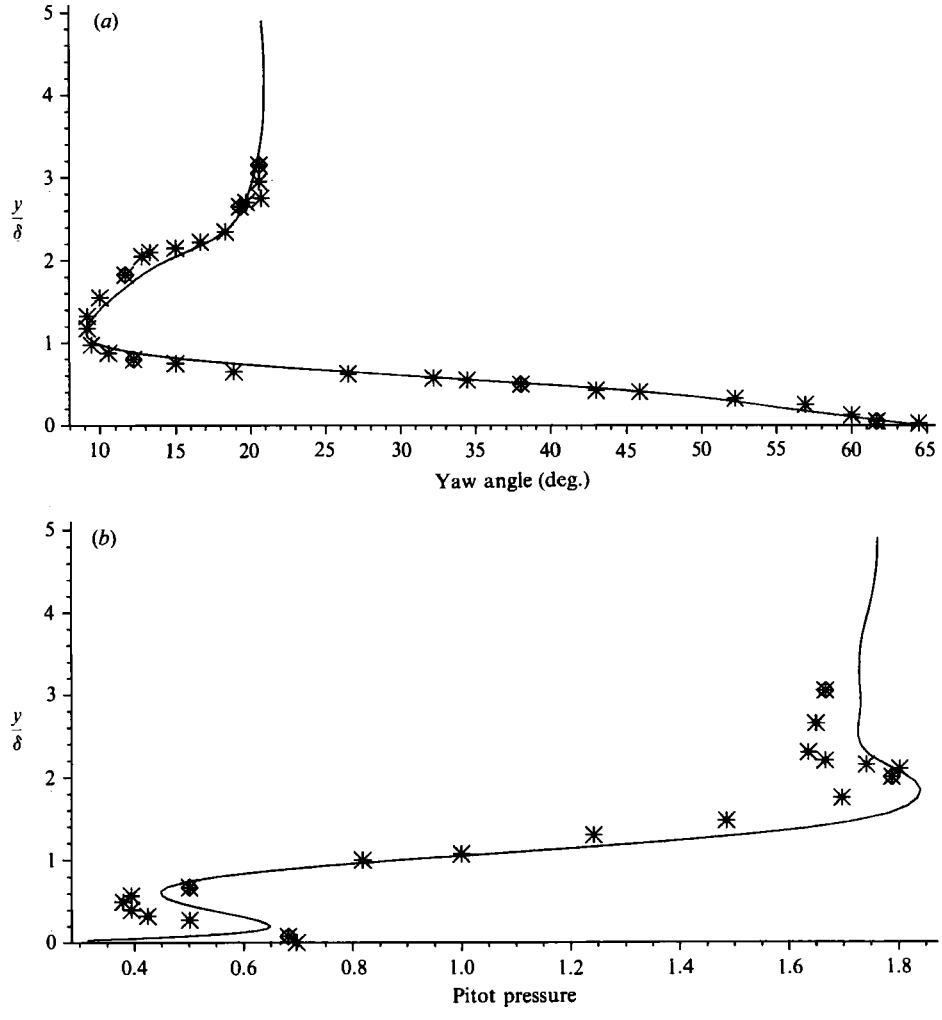

FIGURE 6. Comparison of calculated and measured Pitot pressure and yaw angle at Station 7: (*a*) yaw angle; (*b*) Pitot pressure.

angle. The data at Station 8, which is located $2.5\delta_\infty$ downstream of the shock, are compared in figure 7. Finally, the surface wall pressure is compared in figure 8. The computed pressure distribution is quite similar to the experimental one.

Compared to the calculations of Knight *et al.* (1987), the present results are closer to the experimental data. This is due to the finer grid and probably to the better shock-capturing nature of the upwind numerical scheme which has been used.

3.2. *Visual analysis of the flow field*

A numerical solution provides as an output the values of the various flow variables (velocity components, density, pressure, etc.) at the grid points of the calculation domain. The transformation of these data into images of the flow field which reveal its structure, is the next phase of a numerical simulation. Various processing techniques have been developed for the detection of vortices. The graphic display of the trajectories which follow particles 'released' at the origin of the flow is one classical technique, which among other details, effectively visualizes vortices which

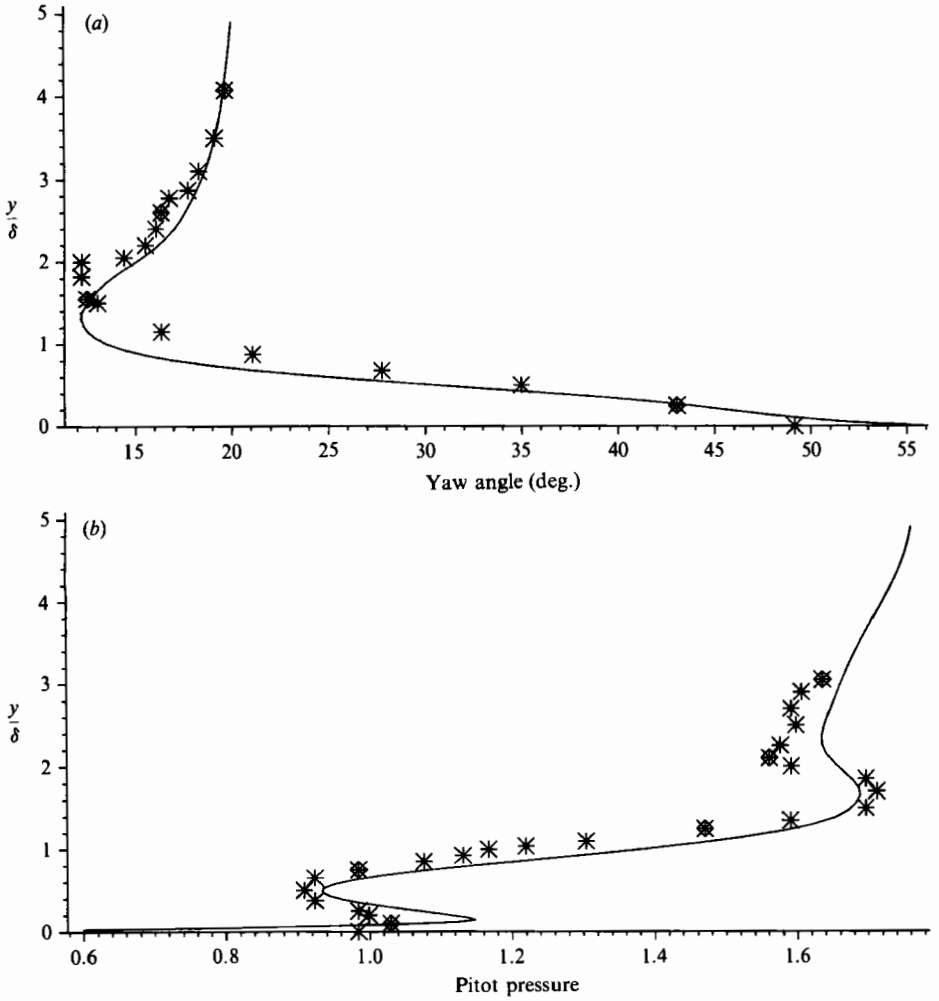

FIGURE 7. Comparison of calculated and measured Pitot pressure and yaw angle at Station 8: (*a*) yaw angle; (*b*) Pitot pressure.

may exist in the flow field. The displayed streamlines turn around the core of the vortices, giving visual evidence of their existence and also an indication of their strength. The calculation of the streamlines is much easier if the region which the vortices occupy at the outflow boundary is known, from experiments or from another method of detection (e.g. from cross-sections of velocity vectors). Then a backward integration of the trajectories provides only the streamlines which are entrained by the vortex. This technique has been applied in this work. However, as a prime visualization tool of the vortices another technique has been used.

An effective technique of automatic detection of vortices in a three-dimensional flow has been proposed by Vollmers Kreplin & Meier (1983). They have shown that vorticity exists in those parts of a flow in which the skew-symmetric part of the rate of strain tensor (spatial derivatives of the velocity field) in non-zero. This skew-symmetric part is related to the curl of the velocity vector field and represents the vorticity. The discriminant of the strain tensor is evaluated numerically at all the points of the flow field. Then contour surfaces of constant values are created and

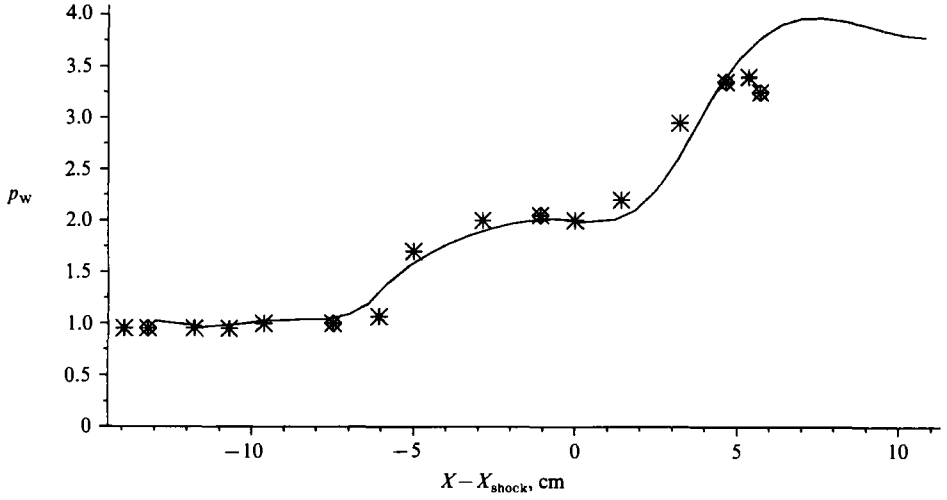

FIGURE 8. Comparison of calculated and measured wall pressure distribution.

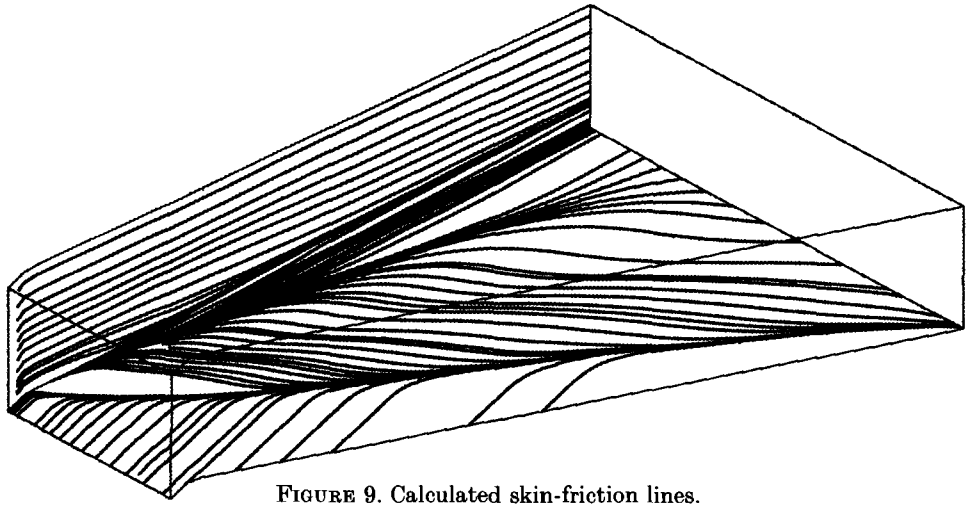

FIGURE 9. Calculated skin-friction lines.

displayed. These contours indicate where in the field there are vortices. The discriminant technique has been incorporated by Vollmers (1989) in a graphic system called Comadi. This system can display simultaneously repeated created images of data. Thus in the same picture vortices and shock waves, for example may be shown though a different technique is used for their graphic detection.

We start the presentation of images of the flow by showing in figure 9 a perspective view of the calculated skin friction lines on the surfaces of the fin-plate configuration. These lines simulate the experimental surface visualization. The skin friction pattern provides first information concerning the flow separation. It is seen in figure 9 that on the flat plate, the separation line originates from the apex of the fin and appears as an asymptote to the skin friction lines which converge towards it. Close to the corner, the reattachment line is formed by the diverging skin friction lines. The distance separating the separation line from the reattachment line increases progressively with the distance from the apex, indicating that the flow is quasi-conical. Close to the apex the separation line is curved, but further downstream it becomes a straight line. This initial region of deviation from conical behaviour is the region called by Lu & Settles (1989) the 'inception zone'.

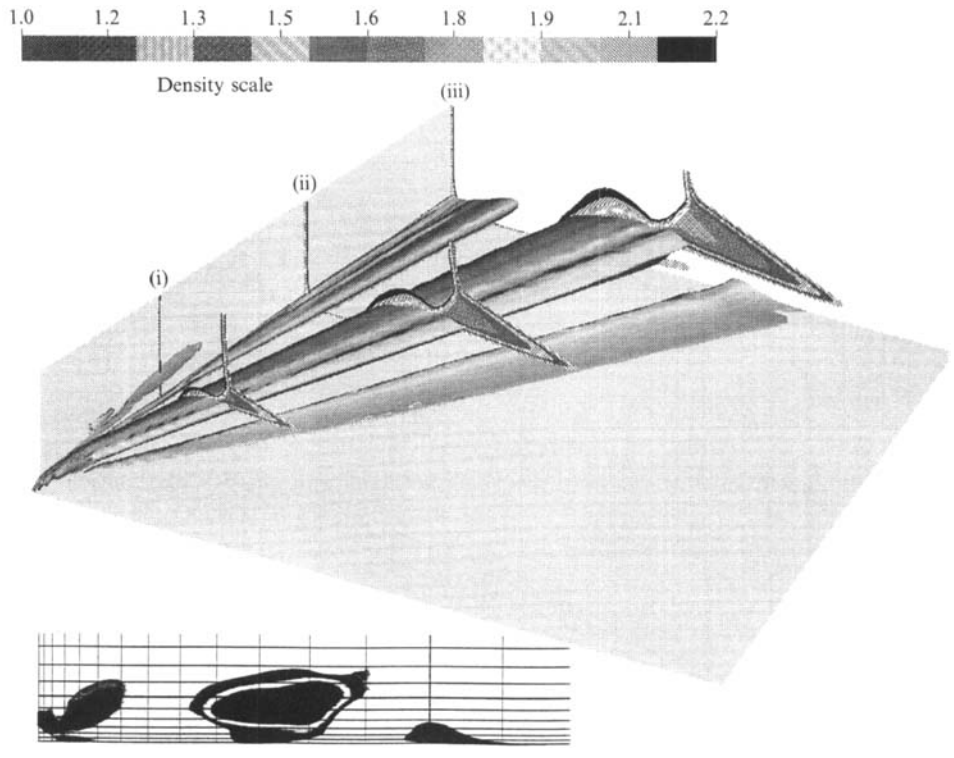

FIGURE 10. Perspective view of the conical vortices and of the shock waves. Vortices are visualized by iso-contours of the discriminant of the velocity gradient tensor, shock waves by iso-contours of the density.

The skin friction lines turn rapidly when they approach the separation line. If the points where the skin friction lines first start to be curved are jointed, the so-called 'upstream influence line' is formed. However, it is not easy to decide on curved lines, like those shown in figure 9, which is the turning point. We have found that this uncertainty is removed if iso-value contours of the wall pressure are used. These contours have been drawn in figure 15. It is seen in this figure that shortly before the rapid turn of the streamlines toward the separation line the shade pattern of the pressure changes from the one which corresponds to freestream values to that which indicates an increase of pressure. The line indicated by this type of visualization is similar to the separation line and it runs close to it, with increasing distance in the downstream direction.

Concerning the fin, it is observed in figure 9 that in its major part the skin friction lines remain parallel to the horizontal plate, but in its lower part, close to the corner, they converge towards a separation line. This line initially moves away from the horizontal plane, however at greater distances from the apex it tends to be parallel to it. On both sides of the corner, on the plate and on the fin, the skin-friction lines are dense, indicating the reattachment region of the longitudinal vortex, which is formed in this area.

The vortices which are expected to appear in this type of flow are shown in figure 10, where the contours of the eigenvalues of the velocity gradient field are shown, along with some cross-sections on which the density contours have been drawn

(detection of shock waves). Figure 10 includes all the critical elements of the fin–plate flow. It is observed that, as expected, the flow is dominated by a large vortical structure, which lies on the flat plate and whose core has a remarkably conical shape with a flattened elliptical cross-section. Also on the flat plate, on the side of the main vortex, a very thin vortex core has developed in the direction of the flow. This is not another independent vortex, but the core of the vorticity sheet which lifts off the surface, along the separation line, and rolls up to form the conical vortex. Along the vertical fin and close to the corner, the longitudinal vortex, mentioned by Kubota & Stollery (1982), is seen. It also develops quasi-conically, but with a smaller rate of increase, compared to the prime conical structure. In the lower part of the figure, a cross-section of the vortices is shown. There it is indicated that indeed the flat ground vortex constitutes the initial part of the primary conical vortex. In addition, it is observed that the fin vortex has contact with the fin itself and with the plate.

The density contours on three cross-sections of the flow (i–iii), which are also displayed in figure 10, visualize very clearly the shock system which is formed along and on top of the conical vortex. The system is composed of the glancing shock wave (which appears owing to the existence of the fin), of the separation shock, produced by the coalescence of the compression waves, and of the rear quasi-normal shock, which extends from the bifurcation point to the surface of the conical vortex.

Some features of the flow field are better visualized if the vorticity is used as a visualization parameter. In figure 11 the vorticity sheet of the boundary layer is shown, appropriately 'illuminated', to give the impression of a three-dimensional picture. In this figure it is clearly shown that the vorticity sheet lifts off the surface of the plate, along the separation line, to form the conical separation vortex. Along the fin and close to the corner the formation of the fin vortex is also clearly shown. Other features of the flow field are shown in figure 12, where the iso-contours of the absolute value of the vorticity have been drawn in two cross-sections of the flow field (sections (ii), (iii) of figure 10). It is seen that in addition to the shock system which has already been visualized by the density contours in figure 10, the shear layer which originates at the triple-point and impinges on the corner is clearly shown. It is noted that the density difference across the shear layer is too small to be visible in the density contours shown in figure 10. A remarkable similarity exists between the cross-section of the flow shown in figure 12 and the model of Alvi & Settles (1990), figure 3, which is based on their shadowgraph pictures.

The distribution of vorticity within the conical vortex is another critical feature of the flow which is shown in figure 12. It is seen that the vortex is continuously fed with the vortical fluid of the boundary layer. Higher values of vorticity are observed on the upper part of the vortex at the cross-section (ii) than at the cross-section (iii). This is clearly indicated in the pictures by the relative size of the black contour. Trying to explain this difference in the vorticity distribution, we note that while the thickness of the boundary layer in section (iii) is slightly larger than the thickness of the boundary layer in section (ii), the size of the vortex is considerably larger in section (iii). Thus, almost the same influx of vorticity is distributed in a larger cross-section in the downstream section (iii). Concerning the circulation around the conical vortex, it is expected that owing to the viscous effects it is decreasing downstream. For estimating the circulation of the vortex at section (ii) or (iii), the numerical calculation of the outflow of vorticity through the cross-section of the vortex is required. Such a numerical integration, on a surface whose border is not clearly defined, will not provide reliable results.

Some other details of the shock system and of the conical vortex are shown in

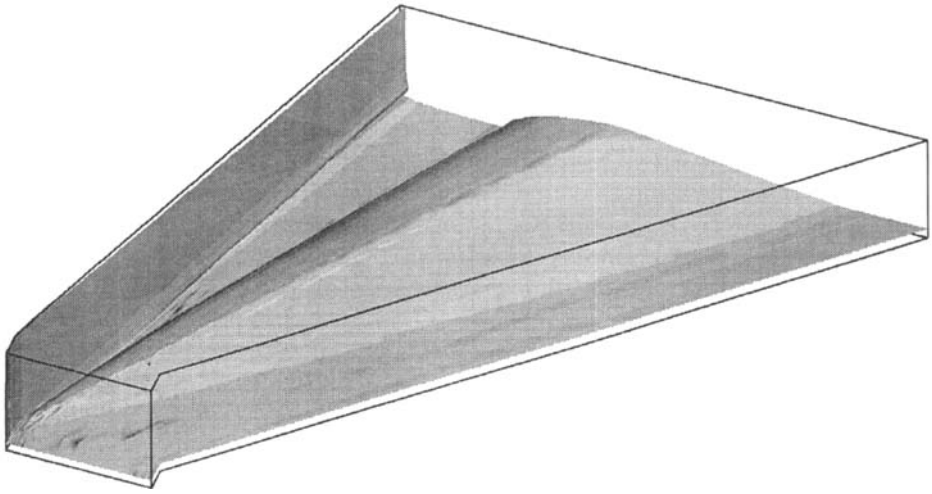

FIGURE 11. Visualization of the vorticity sheet of the boundary layer.

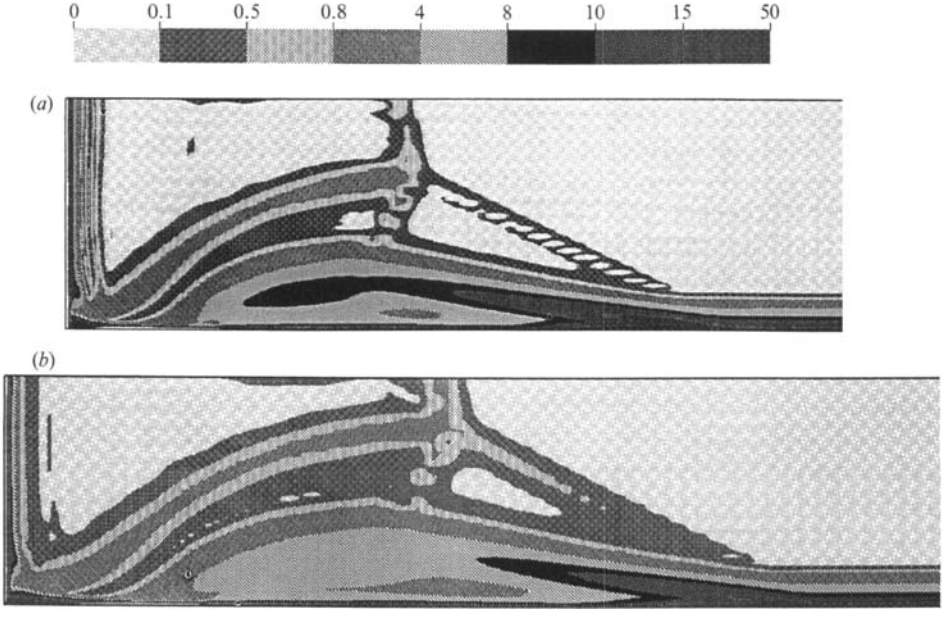

FIGURE 12. Iso-contours of the absolute value of vorticity: (*a*) at section (ii); (*b*) at section (iii).

figure 13(*a*), where the iso-Mach lines and the velocity vectors have been drawn at a cross-section normal to the shock wave at the outflow region. In the same figure the border lines of the vortices have been drawn. It is seen that the core of the conical vortex is located in a region of high shear. No circulatory motion is visible in the corner region where the vorticity distribution indicates the existence of the fin vortex. That is because the axis of this vortex is almost parallel to the fin and not to the glancing shock, like the conical vortex. The fin vortex is visible in figure 13(*b*), where in an enlargement of the corner region the velocity vectors have been drawn at a cross-section normal to the fin.

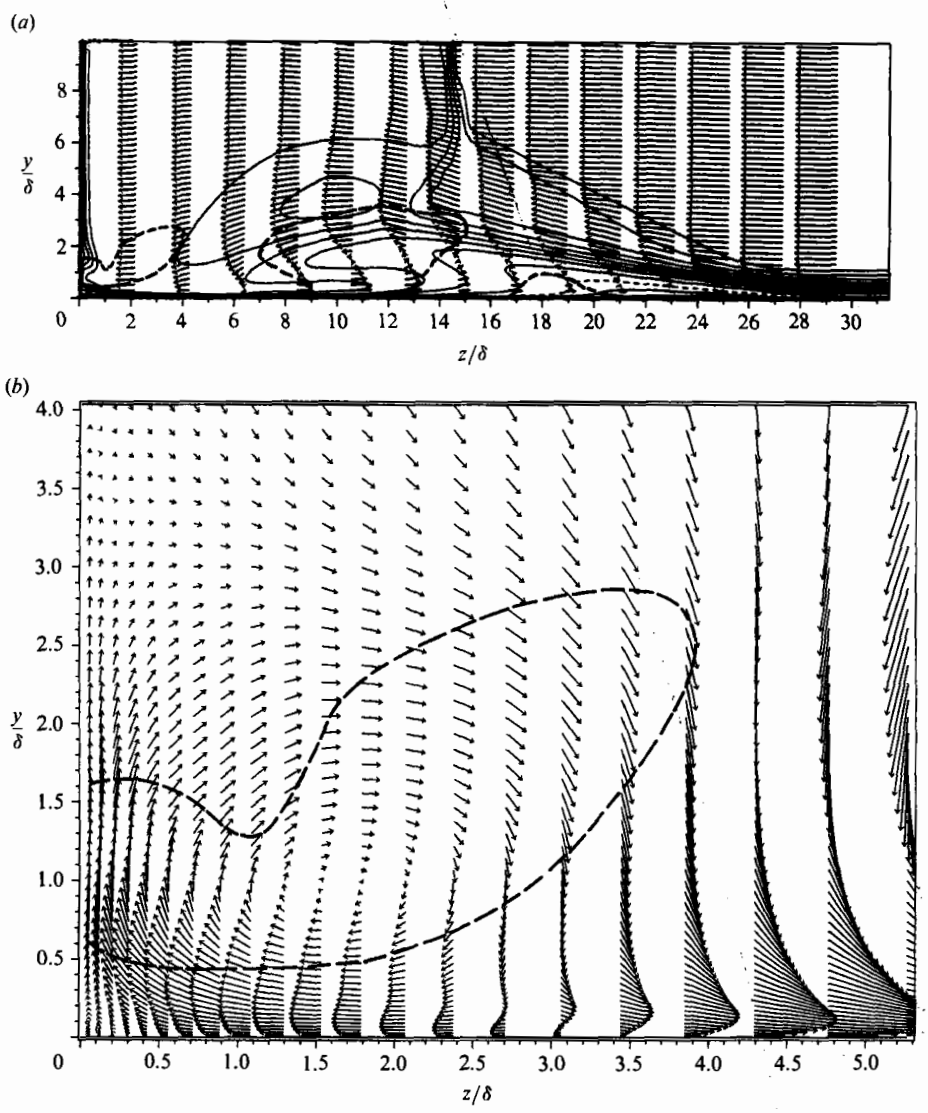

FIGURE 13. (*a*) Iso-Mach lines, velocity vectors and border lines of vortices at a cross-section normal to the glancing shock. (*b*) Velocity vectors and border lines of the fin vortex at a cross-section normal to the fin (enlargement of the corner region).

The induction characteristics of the vortices of the flow field are indicated in figure 14, where some of the streamlines which pass through their cores are shown along with a cross-section of the vortices. It is seen that the conical vortex completes more than one turn in the calculated field, while it is hard to say that the fin vortex turns, in the extent of the field. As expected, the conical vortex rotates in a counterclockwise direction. Coloured streamlines, not included in this paper, indicate that the flat vortex, formed by the lifted off vorticity layer, also rotates very slowly in a counterclockwise direction. Concerning the fin vortex, we suppose that it rotates very slowly in a clockwise direction. This is indicated by the skin-friction lines.

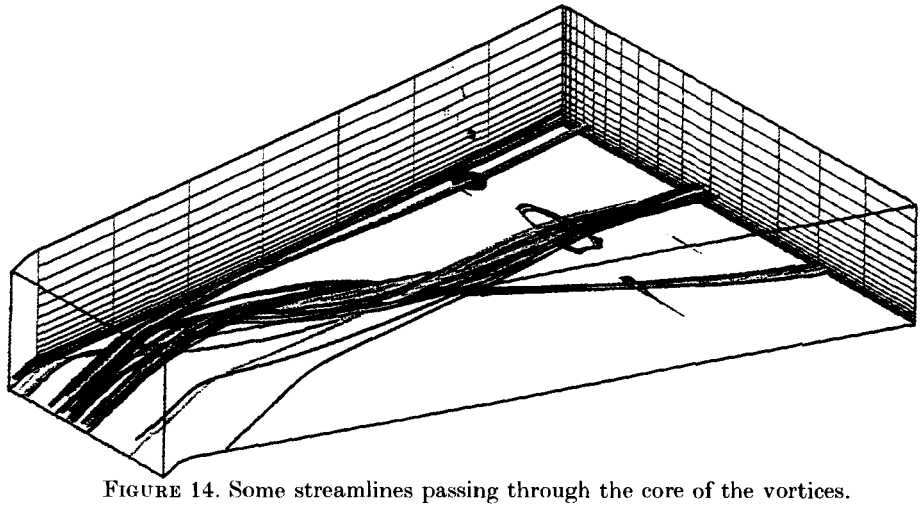

FIGURE 14. Some streamlines passing through the core of the vortices.

3.3. *Determination of the virtual origin of the conical flow*

It has been mentioned already that the existence of a virtual origin, on which all the critical lines of the flow meet, is one of the consequences of the establishment of a conical flow field in a fin–plate configuration. The existence of this origin may be verified if in figure 10 the border lines of the conical vortex and the line which joins the shock triple-point are drawn. Then these three lines meet almost at the same point, upstream of the fin. It is worth noting also that the boundaries of the flat vortex meet approximately at the same point.

A more precise determination of the virtual origin is given in figure 15, where the skin friction lines and the vortices are shown, viewed from below the flat plate. It is seen in this figure that the separation line, the reattachment line and the shock line almost meet at the same point. If the border lines of the vortex are drawn they give a slightly different intersection. This happens because the size of the vortex depends to an extent on the sensitivity value of the function which is used for its visualization. For eliminating possible error caused by the graphical determination of the virtual origin, a numerical search has been done, assuming that the origin lies on the extrapolation of the inviscid position of the shock. During this search, the virtual origin was located at successive positions along the shock line, and at each position the pressure along conical rays was checked to see if it was constant. The best conical behaviour was found when the virtual origin was located a little closer to the fin than the origin determined graphically. This position was used subsequently for studying the conical similarity.

3.4. *Factors which may adversely affect the establishment of a conical flow field*

The existence of a conical similarity among the geometric parameters of the flow field is an indication that most probably the flow characteristics also follow a conical variation, i.e. flow variables remain unchanged along rays which start at the conical origin and pass through the flow field. Some evidence supporting this view has been provided by Settles & Teng (1984). They have shown that application of conical correlation to the surface pressure distribution in the flow about a swept-back corner, results in almost perfect collapse of the data in the complete range of the flow. However, in the course of this study it has been found that the flow is not purely conical in nature. There are physical processes which adversely affect the conical variation of most of the flow variables.

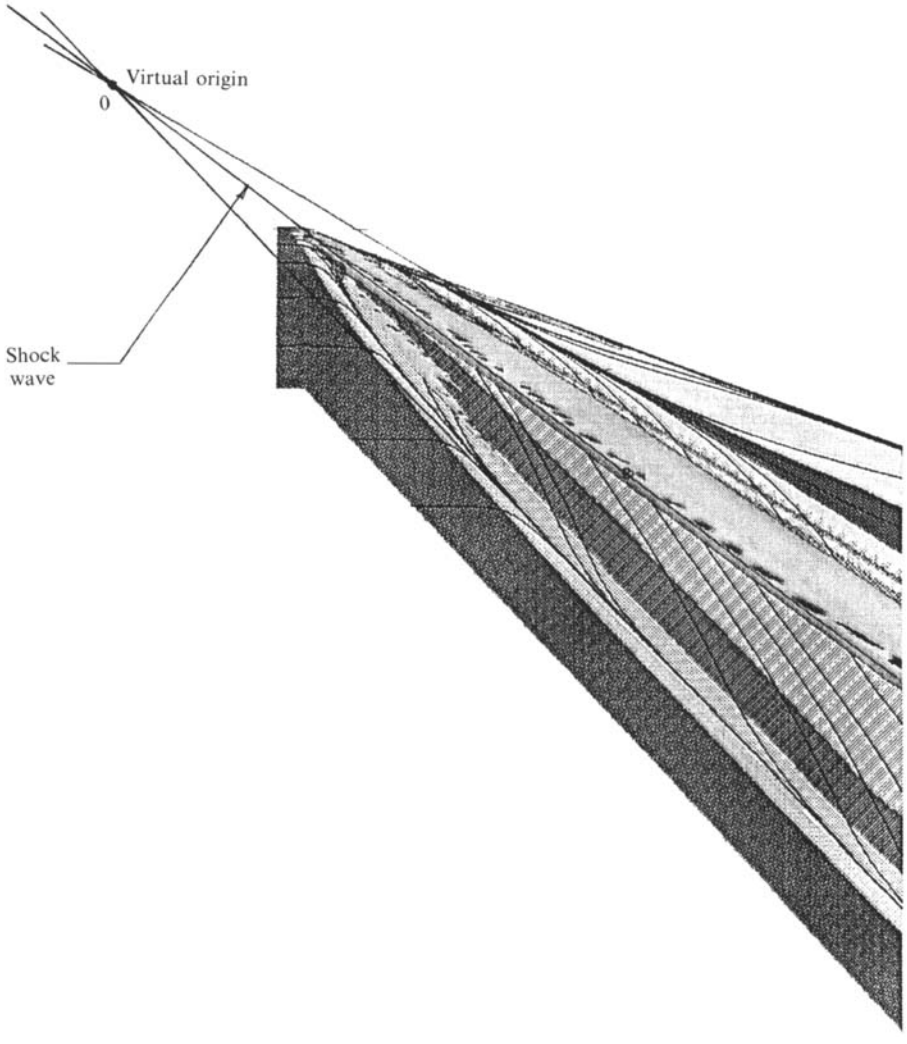

FIGURE 15. Determination of the virtual origin of the conical flow.

Actually, perfect similarity is expected in those cases of conical fields in which the surrounding flow field is uniform. However in the present case the vortex is partially exposed to a non-uniform flow: the boundary layer of the horizontal plate. It is noted that while the vortex at its initial state of development is totally embedded within this boundary layer, gradually it becomes thicker. This happens because the rate of thickening of the boundary layer in the downstream direction is not equal to the rate of increase of the cross-section of the vortex. This feature of the flow field has already been shown in §3.2 (figure 12). Also, from the data of figure 13 it is estimated that the thickness of the vortex at the outflow plane is almost three times greater than the local thickness of the boundary layer. In contrast, we have found that at the end of the inception zone the vortex is just as thick as the boundary layer.

The different rate of thickening of the vortex and of the boundary layer is expected to affect the similarity outside the conical vortex. This statement is supported by the data shown in figure 16(*b*). There, the iso-lines of the Mach number distributions at the first and at the third cross-section of figure 10 have been conically correlated, i.e.

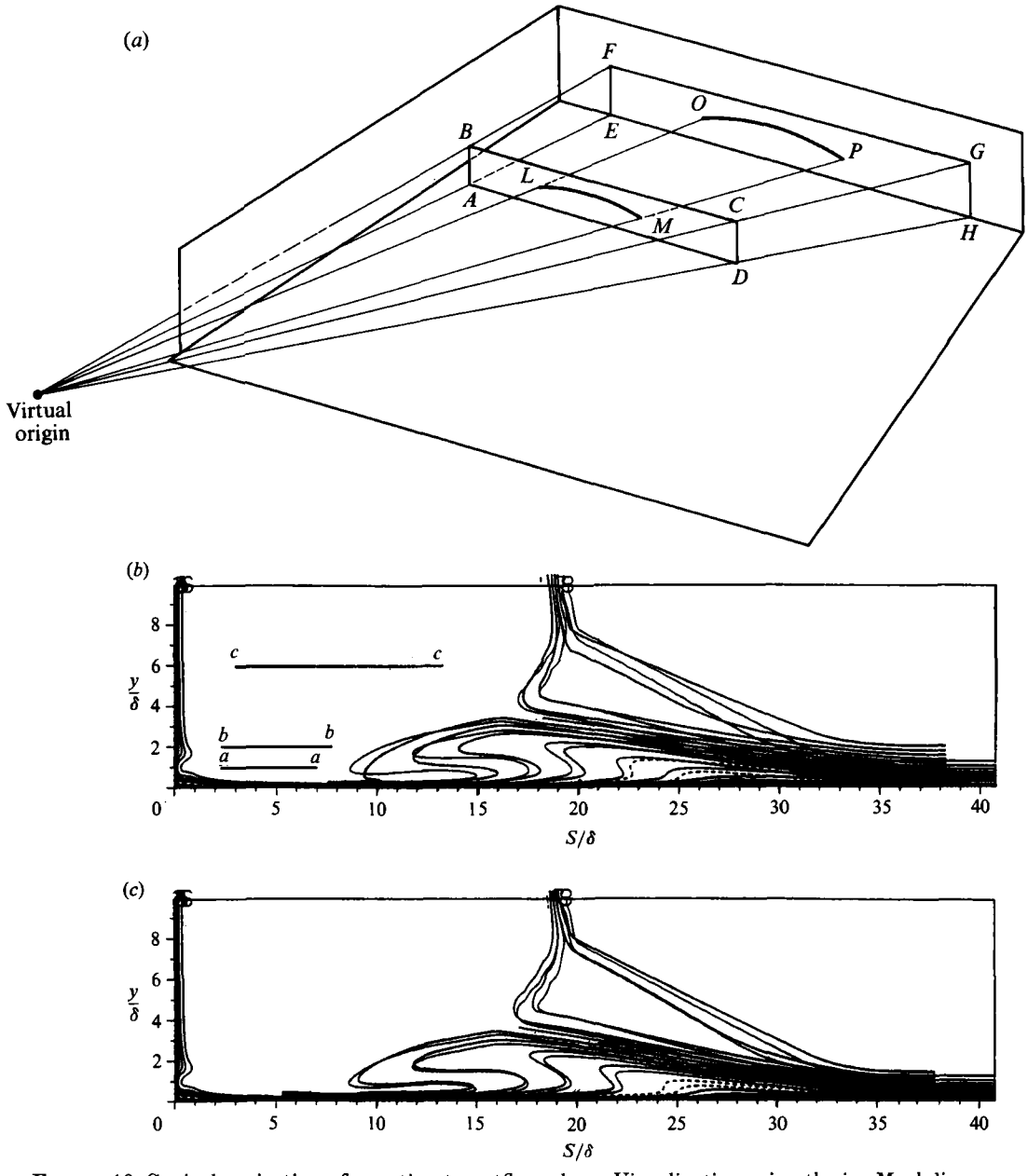

FIGURE 16. Conical projection of a section to outflow plane. Visualization using the iso-Mach lines: (*a*) technique of conical projection; (*b*) projection of section (i); (*c*) projection of section (ii).

the data of the first section has been projected conically on the third. For this, the lengths at the first cross-section were multiplied by 2.07. This is the value of the conical similarity ratio, i.e. the ratio of the distances of the sections from the conical origin. The principles of the conical projection are shown in figure 16(*a*).

If the flow field is purely conical, the iso-Mach lines of the two sections coincide. However, in the present case, while good coincidence is observed between the separation bubbles, the glancing shocks and the triple shock points (figure 16*b*), the feet of the λ-shocks are fairly correlated, especially the separation shocks, while there

is no equivalence at all between the boundary layers in the two cross-sections. More particularly, the boundary layer of the first cross-section is about 40% thicker than the boundary layer of the third section. This large difference in the scaling is due to the lower rate of development of the boundary layer, compared to that of the vortex.

Concerning the similarity of the elements of the λ-shocks, it is observed in figure 16(*b*), that the differences are significant only between the separation shock waves. The rear shocks are closer to each other. The separation shock at the first cross-section forms a smaller angle with the boundary layer than the similar shock at the third cross-section. This is explained if the different thickness of the boundary layer is considered. It has been mentioned in §3.2 that the line which joins the shock triple points passes through the virtual conical origin. The same is valid for the separation line. However the compression lines which form the separation shock start forming at the region of the separation line. Thus returning to figure 16(*b*), in the conically correlated sections the shock–triple points must coincide and the separation shocks must start to form at the same horizontal distance from the fin (equal to about $34\delta_\infty$ in this case). But the vertical distance of origination of the separation shocks depends on the thickness of the boundary layer on each cross-section. In this particular case where the thickness of the boundary layer appears higher in the first section, the separation shock at this station starts at a higher vertical position than the shock at the third station. Hence, its inclination to the horizontal plane will be smaller. In the case of the rear shocks, they are closer, because they start and terminate on parts of the flow which correlate conically very well (the shock triple point and the top of the conical vortex).

The deviations from the conical behaviour are smaller if the two cross-sections which are compared are closer. This is demonstrated in figure 16(*c*), where the second section is conically projected on the third section. In this case the conical similarity ratio is only 1.31. In figure 16(*c*) the projection is very good. Even the thickness of the boundary layers is not very different. It is noted that the second section is located approximately in the middle of the distance of the other sections (see figure 10). The distance between sections (ii) and (iii) is $13.0\delta_\infty$, while between sections (i) and (iii) it is equal to $27.4\delta_\infty$.

The conical projections that were just described may be considered as equivalent to the conical shadowgraphy used by Alvi & Settles (1990). It is remarkable that also in the shadowgraph pictures of Alvi & Settles multiple shock formations exist, one close to the other. Probably they are due partially to misalignment of the shocks, at the initial part of the flow, and partially to the interaction with the boundary layer, as described before.

The increasing value of the angle of the separation shock from the first section to the third, means that the pressure increase through this shock varies similarly. A careful examination of the density contours, in figure 10, shows that indeed the density distribution between the two legs of the λ-shock is not the same at the three sections, but the levels of the values are increasing in the downstream direction. These differences may be interpreted as deviations from the conical similarity. Actually, the different scales of development of the vortex and of the boundary layer have other more severe effects on the conical similarity. In figure 16(*b*), three horizontal line segments (*aa*, *bb*, *cc*) have been drawn. If the flow variables are checked for conical similarity along one of the lines which result if the line segments are extended to the right, for example the middle line segment (*bb*), the following observations may be made. Starting from left to right, the line (*bb*) will cross the vortex and then will pass through the vorticity layer and the boundary layer. While

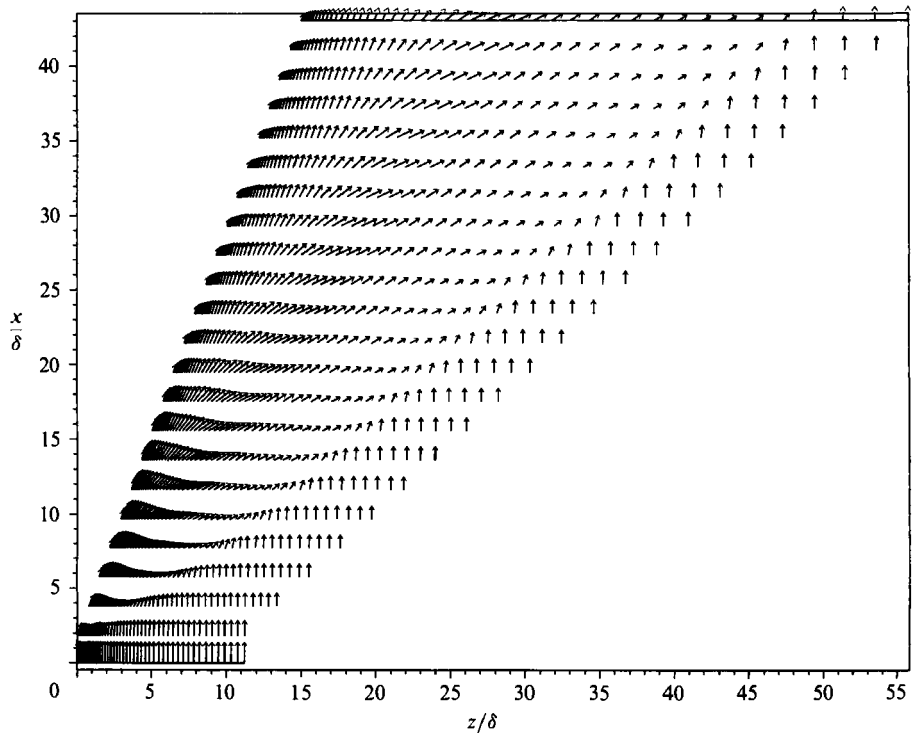

FIGURE 17. Velocity vectors close to the surface of the horizontal plate.

within the vortex the flow conditions are most probably similar, this does not happen within the vorticity layer which envelopes the vortex. That is because owing to the unequal thickness of the undisturbed boundary layers any point of the line will correspond to a different position at the profiles of the two vorticity layers. This is more evident at the right side of the figure. There, the extension of the line segment (*bb*) will be outside the boundary layer of section (iii), but inside the boundary layer of section (i). At any point of line (*bb*) in this region, the various profile variables (velocity, density etc) will have their freestream values at section (iii), but smaller values depending on the shape of the various profiles at the section (i).

If the higher line segment (*cc*) is examined (figure 16*b*), it is found that its extension does not cross the vorticity layers or the boundary layers. Its extension will run through the rear shock and the separation shock. Thus, in this case the possible differences will be related only to the different compression level between the shocks.

The preceding qualitative analysis leads to the conclusion that the flow field as a whole is not purely conical, but a small deviation from conical behaviour exists in a large part of the field. In the next section quantitative data will be presented that will further support this view.

Before proceeding to the quantitative analysis, another possible source of deviation from the conical similarity will be examined: the boundary layer of the fin. This boundary layer starts to be formed at the leading edge of the fin, and it requires some distance to reach a similarity state. In addition, the presence of the fin itself close to the conical vortex may affect its characteristics, at least at the initial part of the flow. Solid support to this statement is provided in figure 17, in which the velocity vectors close to the surface of the plate are plotted. In addition to the developing shape of the boundary layer, the deceleration of the flow close to the fin,

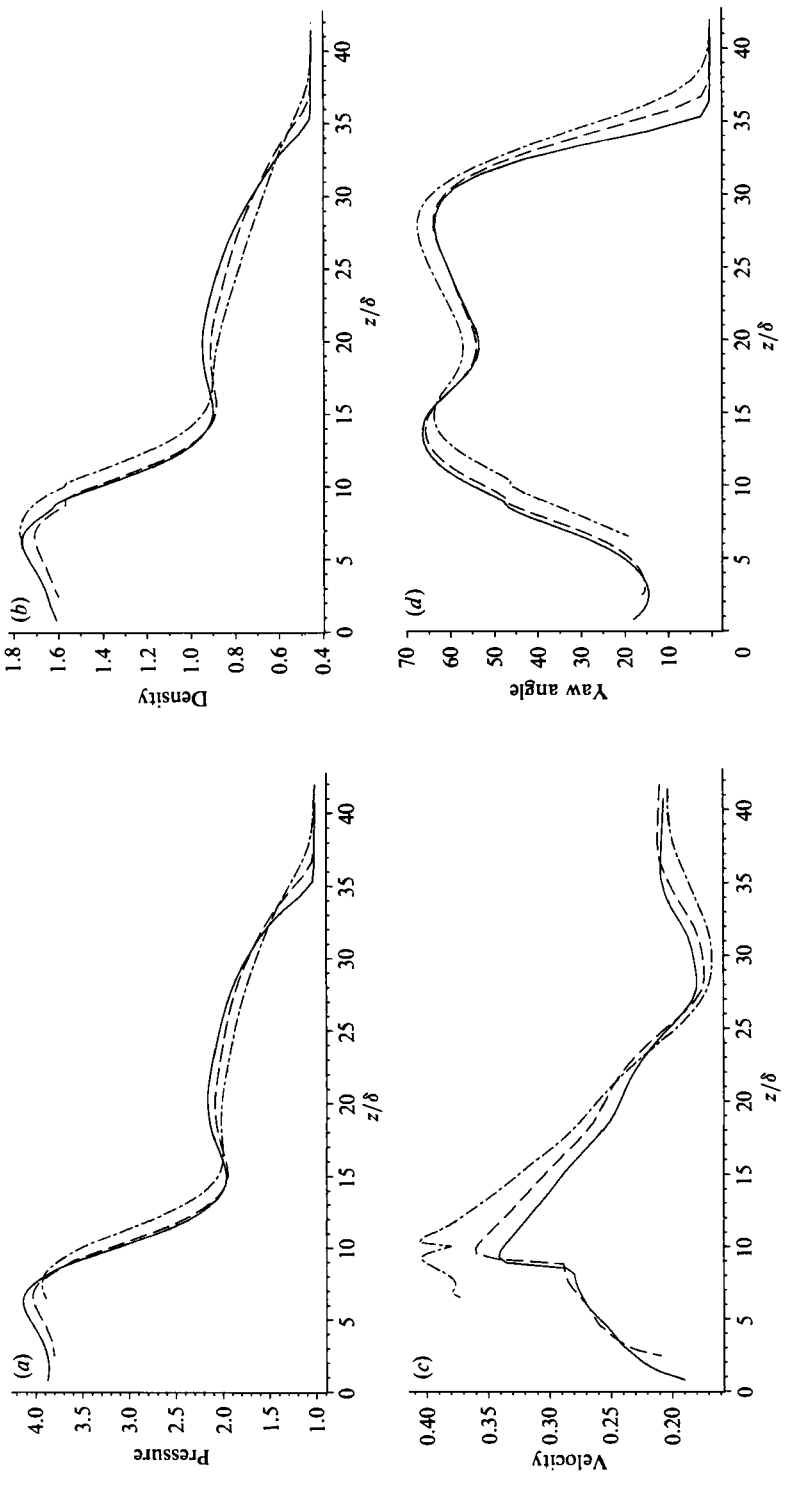

FIGURE 18. Conical correlation of some flow variables parallel to the surface of the plate, near the wall. ——, section (iii); – – –, section (ii); – · –, section (i). (*a*) Pressure; (*b*) density; (*c*) velocity component; (*d*) yaw angle.

at the region where the shock wave interacts with the boundary layer of the plate, is worth noting. The vectors reach a similar profile in the lateral direction at a distance from the fin equal to about $20\delta_\infty$.

3.5. *Quantitative study of the conical nature of the flow field*

In this section the variation of the value of some representative flow variables along conical rays will be presented. The flow variables which will be compared for conical similarity are the pressure, the density, the component of the velocity along the direction of the conical rays and the yaw angle. The comparisons will be done simultaneously at the three cross sections shown in figure 10. Comparisons at four different vertical distances from the plate will be done, i.e. at the wall level (first computational point off it), and at the level of the three horizontal line segments which have been drawn in figure 16(*b*). As before, the data will be conically projected on to the last cross-section.

The distribution of the values of the aforementioned flow variables at the three sections at the level of the wall is shown in figure 18. It is seen in this figure that in the major part of the spanwise extent of the flow field, the pressure and the density show a rather small variation along conical rays which cross the three sections. But some of the effects of the non-uniform field on the conical similarity are visible. Thus, the compression at the region of the separation shock starts earlier in the first section, while the pressure increase is smaller than at the other sections. In the case of the velocity component along the conical rays (figure 18*c*), its variation reflects the distribution of the velocity field (figure 17). The transitional effects have been considerably smoothed out before section (i). Only the curve that denotes the variation of the velocity in this section has a different shape and maximum value from the other curves in the region between the fin and the vortex. Another interesting feature of the flow close to the wall is the observed abrupt increase of the velocity at $z = 9\delta_\infty$, in the case of sections (ii) and (iii), owing to the velocity field of the vortex. The yaw angle (figure 18*d*) has a similar variation at the three sections, but differences in the values exist between the curve of the first section and the other curves.

In figure 19 the distribution of the values at the level of the edge of the initial boundary layer is shown. The pressure is almost the same along the interaction, at the second and at the third section, while the curve which denotes the variation at the first section has smaller values than the other curves. On the contrary, large differences are observed in the variation of the other flow variables along the conical rays. Examining first the density, it is seen that the curves have a spacing between them at the region of interaction of the vortex with the adjacent boundary layer of the plate. Gradually, the curves come closer at the region of the vortex. Evidently, the poor conical similarity is due to the different scale of development of the vortex and of the boundary layer. Actually the curves start from non-equivalent points vertically, owing to the different scales. Different values at the various sections, at the start of the interaction of the shock with the boundary layer are also observed in the case of the velocity. The differences are not so large in the case of the yaw angle (figure 19*d*). It is remarkable to note that the differences between the last two sections are not so large. Evidently, this is due to the small conical similarity ratio. The rather good similarity of the pressure is explained by the fact that the pressure is constant across a boundary layer.

In figure 20 comparisons are done at the height of the vortex core. The pressure, like before, may be considered as following a conical similarity, even in the case of

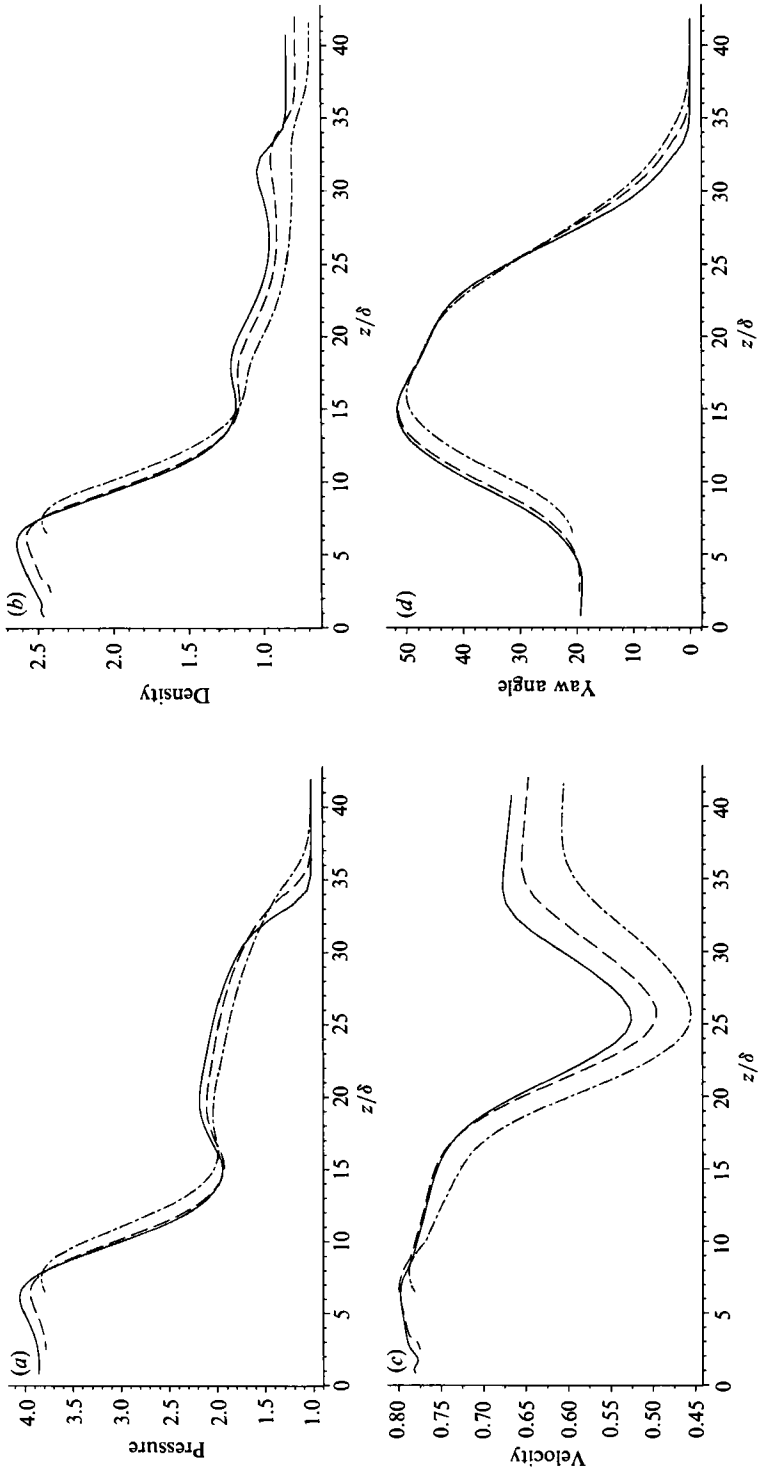

FIGURE 19. Conical correlation of some flow variables parallel to the surface of the plate, at $x = \delta_\infty$, ——, section (iii); – – –, section (ii); – · –, section (i). (*a*) Pressure; (*b*) density; (*c*) velocity component; (*d*) yaw angle.

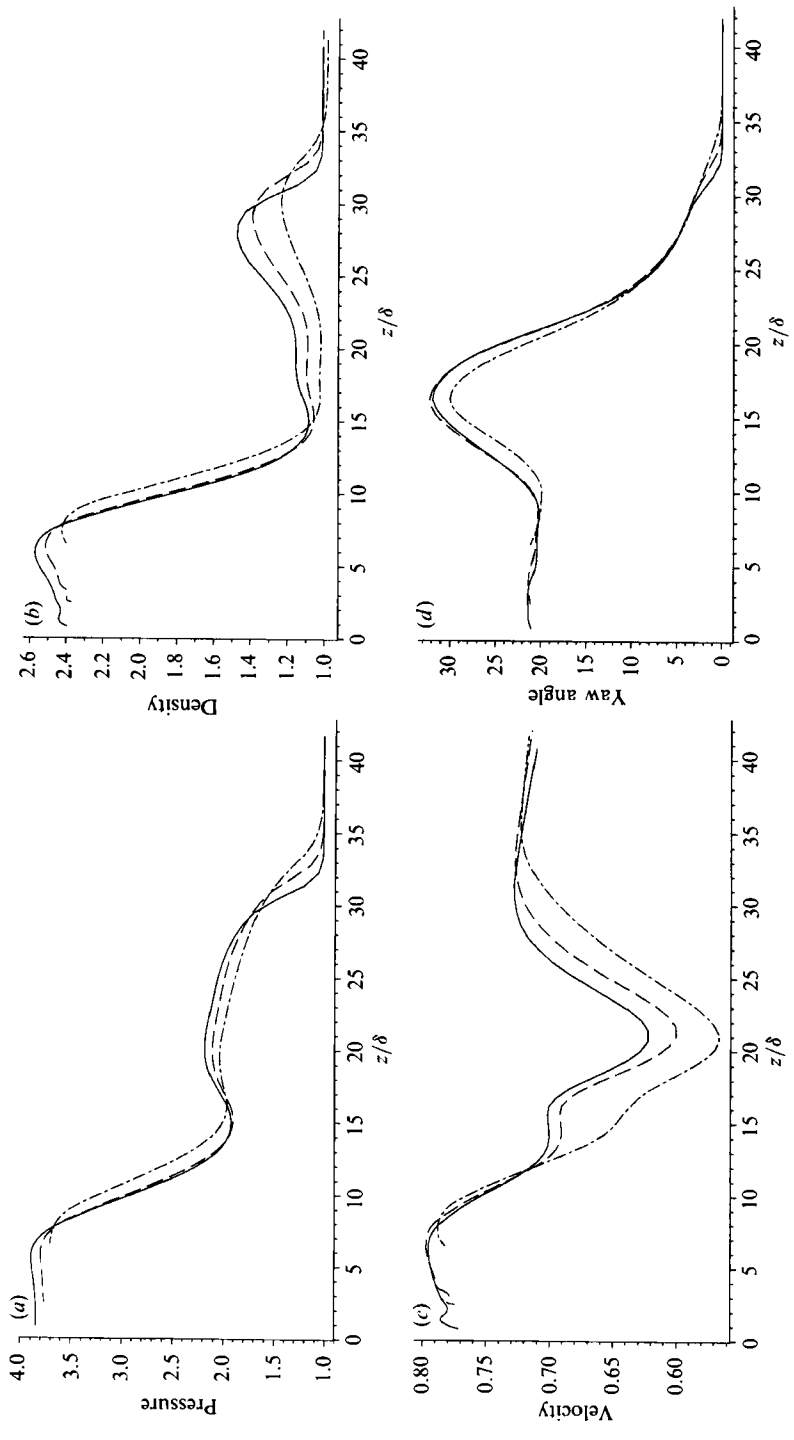

FIGURE 20. Conical correlation of some flow variables parallel to the surface of the plate, at the level of the vortex core. ——, section (iii); – – –, section (ii); – · –, section (i). (*a*) Pressure; (*b*) density; (*c*) velocity component; (*d*) yaw angle.

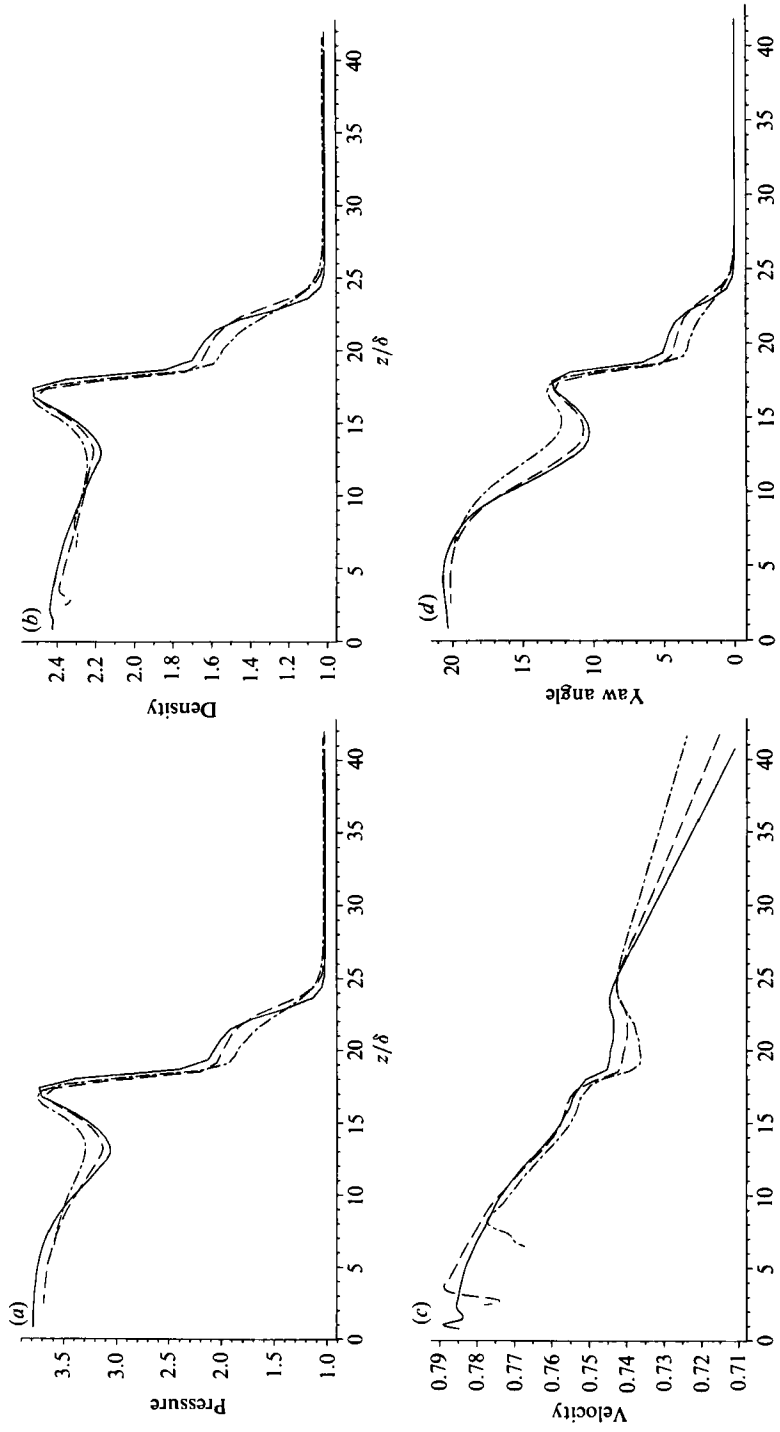

FIGURE 21. Conical correlation of some flow variables parallel to the surface of the plate, below the shock triple point. ——, section (iii); – – – section (ii); – · –, section (i). (*a*) Pressure; (*b*) density; (*c*) velocity component; (*d*) yaw angle.

the first section. But this is not the case for the other flow variables. While the curves denoting the variation at the last two sections are very close, the curves of the first section are much lower for all the examined variables. Especially significant are the differences in the case of the density and of the velocity.

Higher above the vortex, close to the shock triple-point the similarity is improved. A review of the variation of all variables (figure 21), indicates that in the major part of the interaction field the conical similarity is very good. It is only the smaller inclination of the separation shock (see figure 16*b*) at the first section that gives longer interaction length and smaller compression. The agreement at the region of the rear shock is excellent for all the examined variables.

4. Concluding remarks

The supersonic flow about a fin–plate configuration has been simulated numerically, for providing evidence supplementary to experimental studies concerning the nature of the established flow. Field data presented in a graphical form support the flow model proposed by Kubota & Stollery (1982), according to which the flow is dominated by a conical vortical structure which is formed owing to the interaction of the oblique shock generated at the fin with the boundary layer of the plate. Field data presented in a graphical form also support the flow model proposed by Alvi & Settles (1990) according to which the flow is dominated by a shock system consisting of a separation shock and a rear shock, extending from the shock triple-point to the surface of the underlying vortex. For the first time this vortex and a weaker one that appears above the corner, have been visualized in space.

Cross-sections of the flow field have been projected conically at the outflow plane, using the iso-value contours of a flow variable for visualization. It has been found that in reality the flow is not perfectly conical but there are small deviations, especially in the region between the separation shock and the plate. These deviations have been attributed to the different scales of development of the boundary layer of the plate and of the conical vortex. This boundary layer is the one that lifts off the surface and forms the conical vortex. Owing to the different rates of development, the boundary layer at cross-sections far from the outflow plane appears thicker than it should be for a purely conical flow.

As a consequence of the different scales of development of the boundary layer and of the vortex, at a large part of the conical flow field the values of the various flow variables do not remain constant along conical rays but vary slowly. Pressure seems to present a better conical variation than other flow variables, like velocity and density, because pressure is constant across the non-conically developing boundary layer.

The author would like to thank Dr Egon Stanewsky for his invitation to DLR to study the problem of the three-dimensional shock wave/boundary-layer interaction. Also, he expresses his thanks to Dr B. Müller for providing his thin-layer computer code, and to Mr H. Vollmers for his assistance in the preparation of the images of the flow field using the graphic system Comadi and his patience during that cooperation.

REFERENCES

ALVI, F. S. & SETTLES, G. S. 1990 Structure of swept shock wave/boundary-layer interactions using conical shadowgraphy. *AIAA paper* 90-1644.

BALDWIN, B. S. & LOMAX, H. 1978 Thin layer approximation and algebraic model for separated turbulent flows. *AIAA paper* 78-257.

HORSTMANN, C. C. & HUNG, C. M. 1979 Computation of three-dimensional turbulent separated flows at supersonic speeds. *AIAA paper* 79-0002.

HUNG, C. M. & MACCORMACK, R. W. 1977 Numerical solution of supersonic laminar flow over a three-dimensional compression corner. *AIAA paper* 77-694.

HUNG, C. M. & MACCORMACK, R. W. 1978 Numerical solution of three-dimensional shock wave and turbulent boundary-layer interaction. *AIAA J.* **16**, 1090–1096.

KNIGHT, D. D., HORSTMAN, C. C., SHAPEY, B. & BOGDONOFF, S. 1987 Structure of supersonic turbulent flow past a sharp fin. *AIAA J.* **25**, 1331–1337.

KUBOTA, H. & STOLLERY, J. L. 1982 An experimental study of the interaction between a glancing shock wave and a turbulent boundary layer. *J. Fluid Mech.* **116**, 431–458.

LIGHTHILL, M. J. 1963 Attachment and separation in three-dimensional flow. In *Laminar Boundary Layers*. Oxford University Press.

LU, F. K. & SETTLES, G. S. 1989 Inception to a fully developed fin-generated shock-wave boundary-layer interaction. *AIAA paper* 89-1850.

MASKELL, E. C. 1955 Flow separation in three dimensions. *RAE Rep. Aero.* 2565.

MÜLLER, B. 1990 Development of an upwind relaxation method to solve the 3D Euler and Navier–Stokes equations for hypersonic flow. *GAMM Wissenschaftliche Jahrestagung, Hannover, April 1990.*

ROE, P. L. 1981 Approximate Riemann solvers, parameters vectors, and difference schemes. *J. Comp. Phys.* **43**, 357–372.

SHAPEY, B. & BOGDONOFF, S. M. 1987 Three-dimensional shock wave/turbulent boundary layer interaction for a 20° sharp fin at Mach 3. *AIAA paper* 87-0554.

SETTLES, G. S. & DOLLING, D. S. 1986 Swept shock wave/boundary-layer interactions. In *AIAA Progress in Aeronautics and Astronautics: Tactical Missile Aerodynamics* (ed. M. Hemsch & J. Nielsen), vol. 104, pp. 297–379.

SETTLES, G. S. & TENG, H. Y. 1984 Cylindrical and conical flow regimes of three-dimensional shock/boundary-layer interactions. *AIAA J.* **22**, 194–200.

TOKEN, K. H. 1974 Heat transfer due to shock wave/turbulent boundary layer interactions on high speed weapon systems. *AFFDL* TR-74-77.

VOLLMERS, H. 1989 A concise introduction to Comadi. *DLR IB* 221-89 A 22.

VOLLMERS, H., KREPLIN, H. P. & MEIER, H. U. 1983 Aerodynamics of vortical type flows in three dimensions. *AGARD Conf. Proc.* 342, paper 14.

YEE, H. C. & HARTEN A. 1987 Implicit TVD schemes for hyperbolic conservation laws in curvilinear coordinates. *AIAA J.* , **25**, 266–274.